ACS OMEGA

http://pubs.acs.org/journal/acsodf

Article

Functionalized Double Strain-Promoted Stapled Peptides for Inhibiting the p53-MDM2 Interaction

Krishna Sharma, Alexander V. Strizhak, Elaine Fowler, Wenshu Xu, Ben Chappell, Hannah F. Sore, Warren R. J. D. Galloway, Matthew N. Grayson,* Yu Heng Lau,* Laura S. Itzhaki,* and David R. Spring*

Cite This: *ACS Omega* 2020, 5, 1157−1169

Read Online

ACCESS | Metrics & More | Article Recommendations | Supporting Information

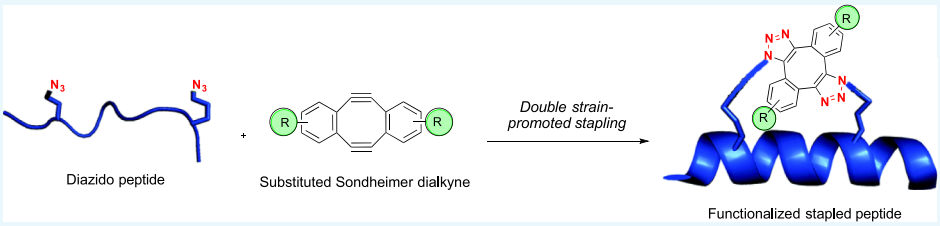

ABSTRACT: The Sondheimer dialkyne reagent has previously been employed in strain-promoted double-click cycloadditions with bis-azide peptides to generate stapled peptide inhibitors of protein−protein interactions. The substituted variants of the Sondheimer dialkyne can be used to generate functionalized stapled peptide inhibitors with improved biological properties; however, this remains a relatively underdeveloped field. Herein, we report the synthesis of new substituted variants of Sondheimer dialkyne and their application in the stapling of p53-based diazido peptides to generate potent stapled peptide-based inhibitors of the oncogenic p53-MDM2 interaction. The functionalized stapled peptide formed from a *meta*-fluoro-substituted Sondheimer dialkyne was found to be the most potent inhibitor. Furthermore, through experimental studies and density functional theory calculations, we investigated the impact of the substituent on the strain-promoted double-click reactivity of Sondheimer dialkyne.

INTRODUCTION

Peptide stapling offers a strategy to generate potent inhibitors of protein−protein interactions (PPIs) by constraining short linear peptides into their native alpha-helical conformation by forming a covalent link between two of its amino acid side chains.[1−6] Recently, a double strain-promoted peptide stapling approach was developed by our group, utilizing a double strained Sondheimer dialkyne reagent **1** (Figure 1a).[7] Sondheimer dialkyne **1** contains two strained alkyne moieties which allow the linking of the two azide containing side chains on the linear peptide in a metal-free environment via a double strain-promoted click chemistry.[8−10] This double strain-promoted stapling approach has been successfully applied to the development of stapled peptide inhibitors of the oncogenic p53-MDM2 PPI, a validated target for anticancer therapeutics.[7] The p53 protein is a tumor-suppressing transcription factor that binds to an E3 ubiquitin ligase protein MDM2 which inhibits the transcriptional activity of p53 and is overexpressed in some cancers.[11−13]

One major general limitation of the double strain-promoted stapling approach is the lack of functional groups on Sondheimer dialkyne **1** and thus the resulting stapled peptides. It was envisaged that the use of substituted Sondheimer dialkynes in the stapling process would allow for the facile introduction of diverse additional functionalities into stapled peptides, which could impart novel physical properties and modify biological activities. To explore this concept, we targeted the design and synthesis of stapled peptide inhibitors of the p53-MDM2 PPI which incorporated substituents on their aromatic ring systems (Figure 1b).

Herein, we describe the synthesis of substituted variants of the Sondheimer dialkyne and their application in the double strain-promoted stapling of a p53 diazo peptide **2** to generate previously unreported functionalized stapled peptide inhibitors of the p53-MDM2 PPI. Substitution was shown to impact significantly upon the biological profile of the stapled peptides, with the pattern of substitution also being of great importance in this regard. In this work, through both experimental and computational studies, we also show how the presence of a substituent on Sondheimer dialkyne influences its azide reactivity in double strain-promoted click chemistry.

Received: October 17, 2019
Accepted: December 24, 2019
Published: January 7, 2020

https://dx.doi.org/10.1021/acsomega.9b03459
ACS Omega 2020, 5, 1157−1169

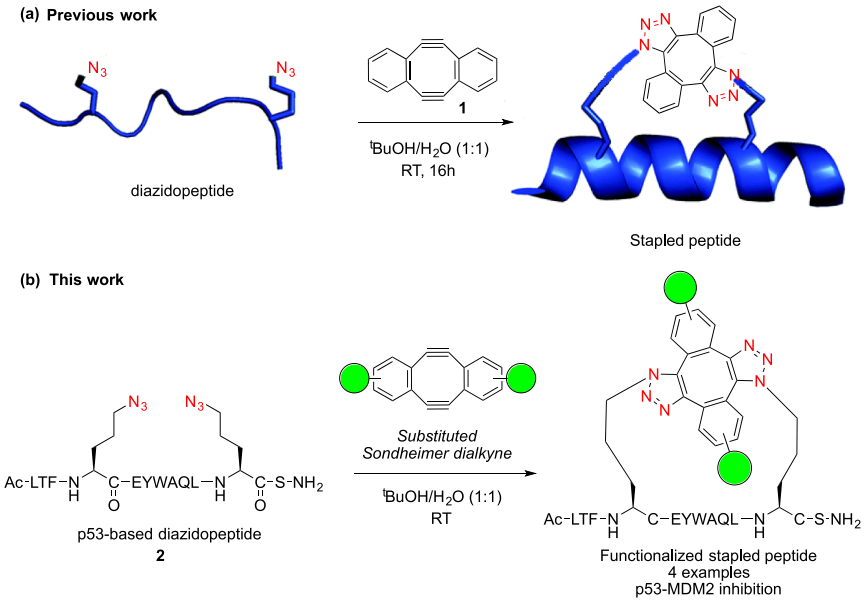

Figure 1. (a) Previous work: use of Sondheimer dialkyne in double strain-promoted stapling of diazidopeptide to generate stapled peptide inhibitors of PPIs. (b) This work: synthesis of functionalized stapled peptides for p53-MDM2 inhibition by application of substituted Sondheimer dialkynes in double strain-promoted stapling of a p53-based diazido peptide.

Scheme 1. (a) Synthesis of Benzyl Sulfone-Substituted Aldehyde Substrates; (b) Synthesis of Substituted Sondheimer Dialkynes

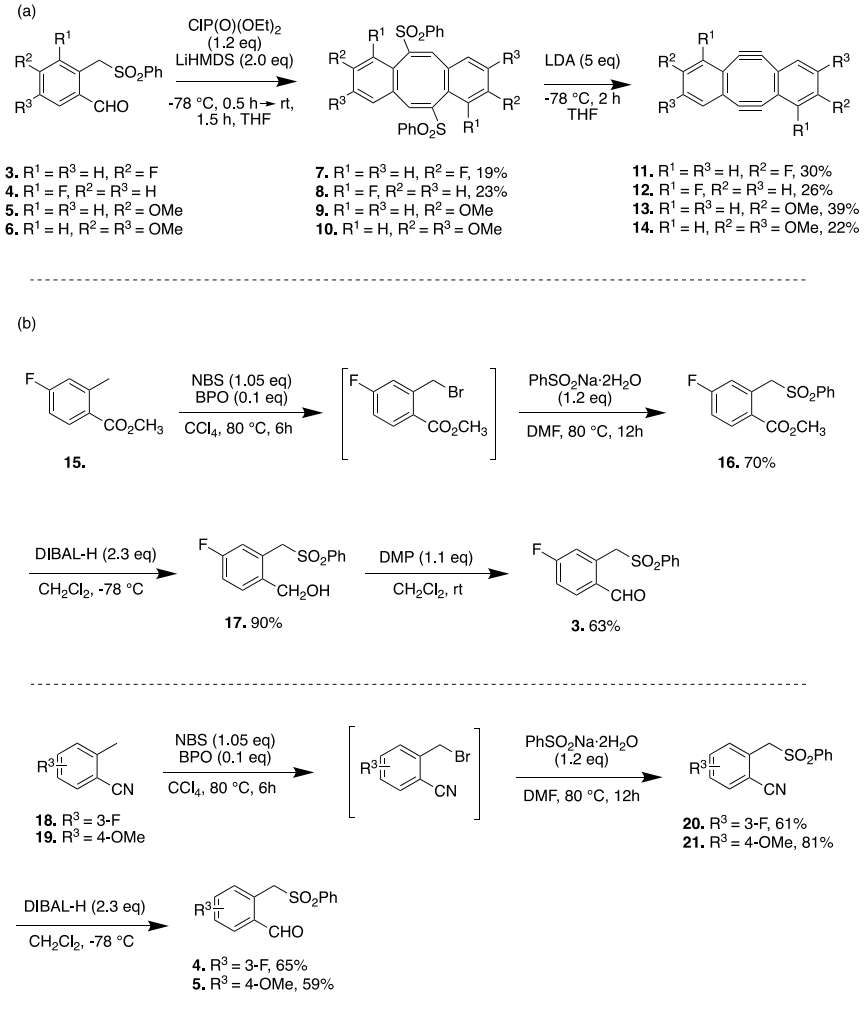

https://dx.doi.org/10.1021/acsomega.9b03459
ACS Omega 2020, 5, 1157−1169

Scheme 2. Application of Fluoro- and Methoxy-Substituted Sondheimer Dialkynes 11−14 in Double Strain-Promoted Stapling of p53-Based Diazidopeptide 2 To Generate Functionalized Stapled Peptide Inhibitors 22−25 of p53-MDM2 PPI[a]

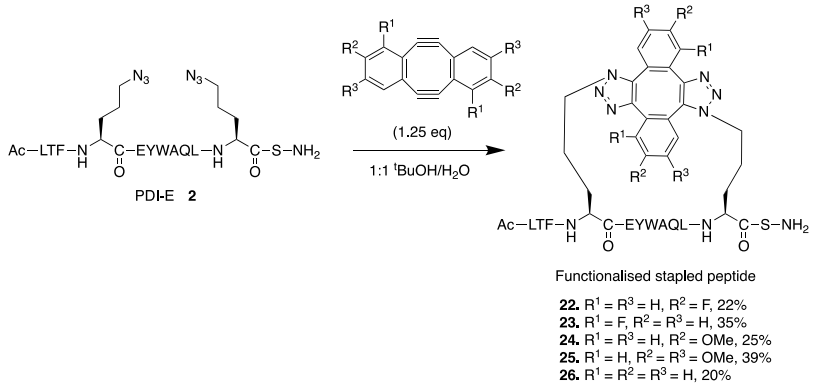

[a]The yields depicted are the isolated yields of the major fraction of the stapled peptides obtained after HPLC purification. The major isomer of the functionalized stapled peptides separated by HPLC purification was tested for biological activity.

RESULTS AND DISCUSSION

Substituted Sondheimer Dialkyne Synthesis. Four different substituted variants of the Sondheimer dialkyne bearing methoxy and fluoro substituents at the meta and ortho-positions relative to the alkyne moiety were targeted (**11**, **12**, **13**, and **14**, Scheme 1a). Orita et al. had previously reported the synthesis of the Sondheimer dialkyne from *ortho*-(phenylsulfonylmethyl)benzaldehyde via a dimerization then double-elimination sequence.[14,15] It was envisaged that this approach could be modified to allow access to the target substituted Sondheimer dialkynes **11**−**14** from the corresponding substituted benzyl sulfone aldehyde substrates **3**, **4**, **5**, and **6** (Scheme 1a).

Substituted benzyl sulfone aldehyde substrates **3**, **4**, and **5** were readily accessed from commercially available starting materials **15**, **18**, and **19** (Scheme 1b). Wohl−Ziegler bromination of *meta*-fluoro-substituted ester **15** and subsequent treatment with benzenesulfinic acid afforded sulfone ester **16**. DIBAL-H reduction of **16** followed by Dess−Martin oxidation gave the desired *meta*-fluoro-substituted aldehyde **3**. The *ortho*-fluoro and *meta*-methoxy substituted sulfones **4** and **5** were synthesized by treating arenes **18** and **19** to Wohl−Ziegler bromination, followed by nucleophilic substitution with benzenesulfinic acid sodium salt. Reduction of the resulting sulfone nitriles **20** and **21** gave the desired aldehydes **4** and **5**. Sulfone **6** bearing a 3,4-dimethoxyphenylsulfonyl group was synthesized by following the reported procedure.[15]

The sulfones **3**−**6** were subjected to Wittig−Horner conditions in the presence of LiHMDS and diethyl chlorophosphate to form the cyclized intermediates **7**−**10** (Scheme 1a).[14] Subsequent treatment with LDA led to the elimination of the phenylsulfonyl groups to afford the desired substituted dialkynes **11**−**14** in low-to-moderate yields. This method was unsuccessful in the preparation of heteroaromatic (pyridine and furan) based variants of Sondheimer dialkyne (see Supporting Information 1.1).

Strain-Promoted Double-Click Peptide Stapling. The substituted dialkynes **11**−**14** were then applied to the double strain-promoted stapling of the p53-based diazido peptide PDI-E **2** (Ac-LTFXEYWAQLXS-NH2, X = Orn(N3))[16,17] in an effort to generate functionalized stapled peptide inhibitors of the p53-MDM2 PPI. Peptide **2** was chosen for stapling as previous work within our group has shown that the stapled peptide generated from PDI-E peptide and Sondheimer dialkyne **1** is a potent inhibitor of the p53-MDM2 interaction.[7] Double strain-promoted stapling of peptide **1** with substituted dialkynes **11**−**14** proceeded successfully to deliver the corresponding functionalized stapled peptides **22**−**25** in 22−39% yield (Scheme 2).The functionalized stapled peptides are drawn as a single isomer for simplicity. These functionalized stapled peptides were then tested for their in vitro binding affinity with MDM2 in a competitive fluorescence polarization (FP)[2,18] assay. The *meta*-fluoro derivative **22** (17.3 ± 7.7 nM) and *meta*-methoxy derivative **24** (8.5 ± 1.9 nM)-functionalized stapled peptides were found to be particularly potent binders of MDM2 (Table 1).

Table 1. In Vitro Binding Affinity of Functionalized Stapled Peptides for MDM2 by Fluorescence Polarization

functionalized stapled peptide	K_d (nM)
22	17.3 ± 7.70
23	501 ± 107
24	8.50 ± 1.90
25	130 ± 28.3

Next, the p53-MDM2 inhibitory activities of the functionalized stapled peptides **22**−**25** in a p53 reporter cell-based assay were evaluated.[18] p53 reporter cells taken in a 96-well format were treated with purified stapled peptides **22**−**25** in Dulbecco's modified Eagle's medium (DMEM) (Figure 2a). The *meta*-fluoro-functionalized peptide **22** was found to be the most potent inhibitor. Moreover, **23** and **24** were also found to exhibit slight inhibitory activity. p53 activation values are reported as fold activation over the activation value obtained when cells were treated with 1% dimethyl sulfoxide (DMSO). This provides an indirect comparative measure of the cellular p53 levels, where higher values are indicative of increased cellular activity. We also performed an in situ stapling assay where p53 reporter cells taken in a 96-well format were treated with linear diazido peptide **2** and substituted dialkynes **11**−**14** in DMEM. This in situ stapling technique allowed the screening of the resultant stapled peptides directly in the cellular medium and avoided the need to perform separate stapling reactions and purifications with each dialkyne variant. This assay also showed *meta*-fluoro-functionalized peptide **22** (fold activation: 3.9 ± 0.7) to be the most potent and twice as active than unsubstituted

https://dx.doi.org/10.1021/acsomega.9b03459
ACS Omega 2020, 5, 1157−1169

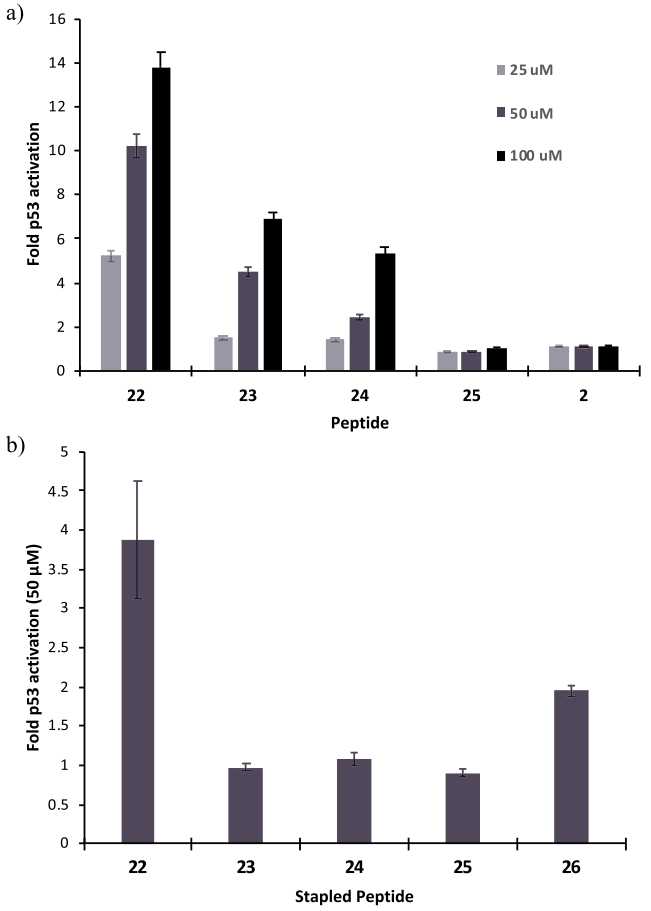

Figure 2. (a) p53 activation in the cellular reporter assay with prestapled purified peptides **22**–**25**. (b) p53 activation in a cellular reporter assay for in situ stapling of **2** (50 μM) with substituted dialkynes **11**, **12**, **13**, **14**, and dialkyne **1** (0.5 mM) in parallel, giving stapled peptides **22**, **23**, **24**, **25**, and **26**, respectively (performed as technical triplicate). Data is reported as fold activation over 1% DMSO.

stapled peptide **26** (fold activation: 1.9 ± 0.1, Figure 2b). No p53 activation was observed with dialkynes **12**, **13**, and **14**.

Kinetic Analysis. To determine the effect of substitution on the azide-reactivity of Sondheimer dialkyne **1**, we experimentally investigated the SPAAC reactivity of our substituted Sondheimer dialkynes bearing substituents at ortho- and meta-positions relative to the alkyne moiety (Figure 3). We studied the reaction kinetics of **11** and **12** by monitoring their consumption in a SPAAC with benzyl azide in methanol using UV spectroscopy (see Supporting Information 1.4 for details). We also compared the kinetic data of *ortho*- and *meta*-amine-substituted dialkynes **27**–**32**, available from our previous studies (Figure 3, see Supporting Information 1.4 for details).[19] The second-order rate constants determined experimentally are depicted in Figure 3.

We observed that the presence of a substituent at the ortho-position led to a significant decrease in the rate of reaction of **1**. A fluoro-substituent at the meta-position (**11**, 0.047 M^{-1} s^{-1}) did not have any considerable effect on the rate of reaction of **1**. On the other hand, a fluoro-substituent at the ortho-position (**12**, 0.004 M^{-1} s^{-1}) resulted in about ten-fold decrease in the rate of reaction compared to **11** and **1**. Moreover, the presence of a larger dimethylamine substituent ortho to the alkyne (**30**) led to a further decrease in reactivity, making it essentially unreactive toward benzyl azide at rt.[19] Similarly, dialkynes bearing a charged trimethylammonium substituent at the ortho-position (**31** and **32**) were also found to be unreactive.[19] Overall, trimethylammonium-substituted dialkyne **29** was found to be the most reactive dialkyne exhibiting 3.6-fold increase in reactivity over Sondheimer dialkyne **1**.

X-ray Crystallographic and Computational Analysis. In order to understand the observed contrast in reactivity between the ortho and meta-substituted dialkynes, we successfully determined the X-ray crystal structures of amine-substituted dialkynes **27**, **28**, **29**, and **30** (Figure 4a). Previously, Bertozzi and co-workers have demonstrated how alkyne bond angles in strained cyclooctyne reagents can be used as a measure to predict their reactivity.[20] Hence, we sought to determine how the presence of different substituents at ortho and meta-position would affect structural changes in our substituted Sondheimer dialkynes. Alkyne bond angles measured experimentally via X-ray crystallography for **27**–**30** are depicted in parenthesis in Figure 4b. From the resulting structural data obtained, we noted

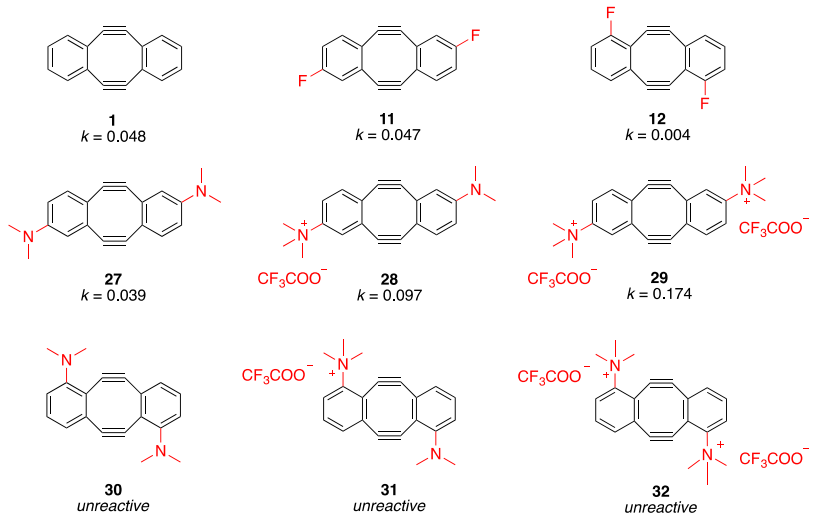

Figure 3. Experimentally determined second-order rate constants (k, in M^{-1} s^{-1}) of substituted Sondheimer dialkynes in SPAAC with benzyl azide in MeOH at rt.

https://dx.doi.org/10.1021/acsomega.9b03459
ACS Omega 2020, 5, 1157−1169

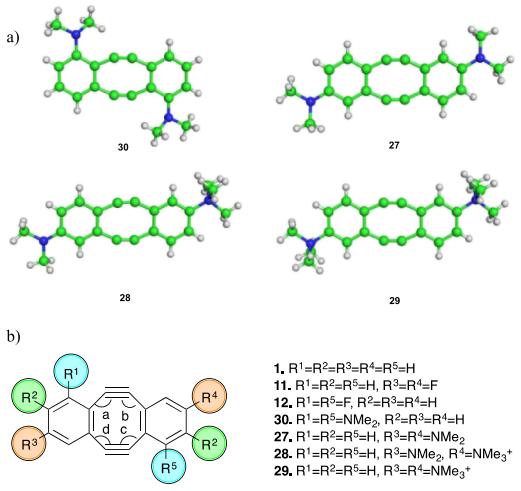

Dialkyne	angle a (°)	angle b (°)	angle c (°)	angle d (°)	Strain energy (kcal mol^{-1})
1	155.5 (156.4)	155.5 (155.3)	155.5 (155.3)	155.5 (155.3)	29.6
11	155.6	155.3	155.6	155.3	29.6
12	154.0	156.3	154.0	156.3	29.9
30	156.1 (156.3)	155.9 (156.5)	156.1 (156.3)	155.9 (156.5)	29.8
27	155.8 (156.3)	154.8 (155.2)	155.8 (156.3)	154.8 (155.2)	28.9
28	156.8 (158.6)	153.8 (153.1)	154.8 (154.5)	155.9 (156.9)	28.3
29	155.7 (155.5)	154.9 (156.3)	155.7 (155.5)	154.9 (156.3)	27.6

Figure 4. Structural analysis of substituted Sondheimer dialkynes. (a) X-ray crystal structures of dialkynes **27**, **28**, **29**, and **30**. (b) Calculated bond angles and strain energy values (X-ray crystallography data shown in parenthesis).

that the presence of a dimethylamine substituent at either the ortho or meta-position (**30** and **27**) did not affect any significant structural change on Sondheimer dialkyne **1** (Figure 4b). A charged trimethylammonium substituent (**28**) at the meta-position, however, did affect minor structural changes on the dialkyne distorting the alkyne bond angles slightly, reflecting an increased reactivity.

Concurrently, we also performed a computational analysis to predict the alkyne bond angles of our amine and fluoro substituted dialkynes **11**, **12**, **27**−**30** (Figure 4b). All geometry optimizations were performed using Gaussian 09[21] with the B3LYP density functional and the 6-31G(d) basis set within the CPCM model for methanol as the solvent at standard conditions (see Supporting Information 2 for full computational details).[8,20,22,23] Single-point energies were calculated using M06-2X,[24] the polarized, triple-ζ valence quality def2-TZVPP basis set of Weigend and Ahlrichs,[25] and an ultrafine integration grid within the CPCM model (methanol). The Gibbs free energy values were determined by the addition of the B3LYP thermal correction to the M06-2X energies.[26] This approach has previously been shown to give reliable results when modeling organic reactions.[27,28] The computationally obtained geometry optimized structures of the substituted dialkynes **27**−**30** corroborated with the X-ray crystal structures (see Supporting Information 1.5 and 2.1.1 for details). Furthermore, these studies indicated that the presence of a fluoro substituent at the ortho or meta-position (**12** and **11**) did not result in any significant structural change on Sondheimer dialkyne **1** (Figure 4b). We also calculated the strain energies for these substituted Sondheimer dialkynes in accordance with the work previously reported by Orita and co-workers (Figure 4b, see Supporting Information 2.2 for details).[15] We found that all of the substituted dialkynes show similar values of strain energy.

Generally, we noted that the substitution of Sondheimer dialkyne **1** did not result in any significant structural change and all substituted dialkynes demonstrated alkyne bond angles around 155°, along with similar strain energy values. This suggested that alkyne bond angle distortion and strain energy are not the sole factors determining the reactivity of these substituted strained alkynes and that there are other potential factors like steric and electronic effects playing a role.

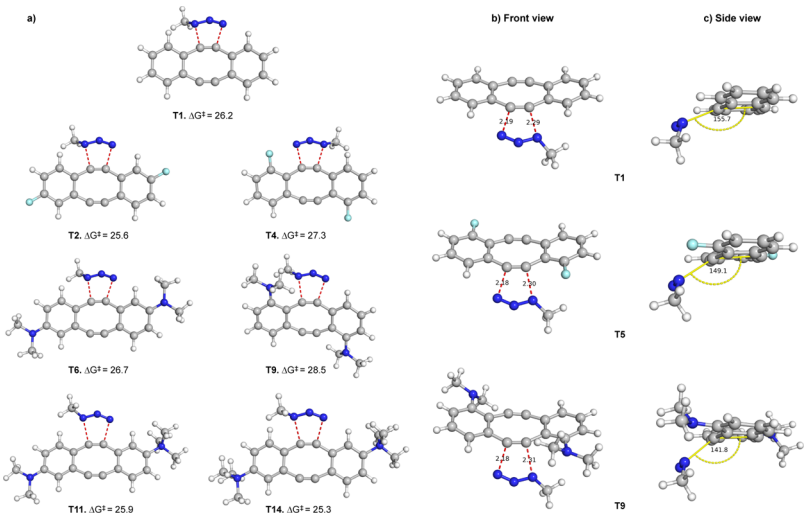

Figure 5. (a) Transition-state structures and activation free energies in kcal/mol for cycloaddition of substituted Sondheimer dialkynes with methyl azide in methanol. (b) Front view of the transition states of cycloaddition with dialkynes **1**, **12**, and **30** depicting C−N bond lengths. (c) Side view of the transition states depicting the angle of the azide approach during cycloaddition with dialkynes **1**, **12**, and **30**.

https://dx.doi.org/10.1021/acsomega.9b03459
ACS Omega 2020, 5, 1157−1169

Therefore, to further investigate the effect of the substituent on the reactivity of our amine and fluoro-substituted Sondheimer dialkynes **11**, **12**, **27**−**30**, we calculated their transition state barriers in a SPAAC with methyl azide (Figure 4a). Previously, Goddard and co-workers have computationally predicted a decrease in reactivity for dibenzocyclooctynes over cyclooctynes due to the resulting steric interference between the incoming azide and hydrogen atom on the benzene ring ortho to the alkyne.[29] A similar decrease in the reactivity in the presence of an ortho-substituent has also been observed by Bertozzi and co-workers with biarylazacyclooctynone (BARAC)-based alkynes.[20]

We started our investigations with Sondheimer dialkyne **1** and calculated the transition states for both first and second cycloaddition with methyl azide in MeOH at rt. We chose methyl azide as it is less conformationally flexible than benzyl azide, and calculations show that it behaves similarly to benzyl azide in a SPAAC with **1**.[20] We found that the first cycloaddition leading to the formation of the monoyne intermediate is the rate-determining step because the second cycloaddition demonstrated a lower activation energy barrier than the first (by 3.6 kcal/mol, see Supporting Information Figures S86 and S94 for details). This is in accordance with the results obtained by Hosoya and co-workers for the SPAAC of Sondheimer dialkyne **1** with methyl azide.[8] Therefore, we calculated the transition states and activation barriers of the first cycloaddition for all of our substituted Sondheimer dialkynes (Figure 5a). Transition states were found for both *anti*- and *syn*-attack (see Supporting Information 2.1.3 for details) of methyl azide on dialkynes, we denote here the one with the lower activation barrier for rate comparison.

We found that substitution of Sondheimer dialkyne with a fluoro group at the meta-position **11** led to a small decrease in the activation barrier (by 0.6 kcal/mol), whereas substitution with dimethylamine at meta-position **27** led to a small increase in the activation barrier (by 0.5 kcal/mol). However, substitution with either a fluoro **12** or dimethylamine **30** at the ortho-position led to large increments in the activation barrier (by 1.1 and 2.3 kcal/mol, respectively), thereby suggesting a decreased SPAAC reactivity. This increase in the SPAAC activation barrier of Sondheimer dialkyne in the presence of an ortho-substituent was found to be more significant with the bulkier dimethylamine substituent **30** in comparison to fluoro **12**. This was clearly reflected in their relative SPAAC rates observed experimentally (Figure 3).

We further analyzed the transition states of ortho-substituted dialkynes **12** and **30** in order to explain their observed inactivity (Figure 5b,c). This demonstrated that the presence of a bulkier dimethylamine substituent in **30** leads to an increased C−N bond distance (by 0.2 Å) on one side in the transition state (Figure 5b). This is consistent with the observation made by Bertozzi and co-workers with ortho-substituted BARAC.[20] The presence of a relatively smaller fluoro substituent at the ortho-position in **12** similarly resulted in a small increase in the C−N bond distance (by 0.1 Å). We also looked at the approach of the methyl azide toward dialkynes **12** and **30**, and we noticed from the transition states (side-view) that as the size of the ortho-substituent increases, the angle of attack (from the plane of dialkyne) increases (Figure 5c). These observations confirm that the presence of an ortho-substituent on Sondheimer dialkyne hinders the approach of methyl azide during cycloaddition, and the larger the substituent the more significant is the effect. Conversion of *meta*-dimethylamine-substituted dialkyne **27** to monocharged **28** led to a decrease in the cycloaddition barrier (by 0.8 kcal/mol), suggesting an increase in rate of reaction (Figure 6a). This was further decreased (by 0.6 kcal/mol) on conversion to the bis-charged **29,** suggesting a further increase in the reactivity. This was in accordance with their relative rates of reaction observed experimentally.

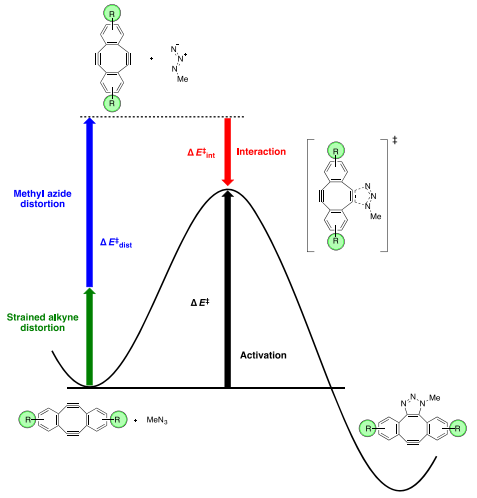

b)

Dialkyne	$\Delta E^{\ddagger}_{dist}$ (kcal/mol)	$\Delta E^{\ddagger}_{int}$ (kcal/mol)	$\Delta E^{\ddagger}$ (kcal/mol)	$\Delta G^{\ddagger}$ (kcal/mol)
1	23.7	-10.3	13.4	26.2
11	23.7	-10.7	13.0	25.6
27	23.8	-9.6	14.2	26.7
12	25.0	-10.7	14.3	27.3
30	25.5	-10.3	15.2	28.5

Figure 6. (a) Application of D/I analysis on SPAAC of methyl azide with substituted Sondheimer dialkynes. (b) Table depicting calculated distortion energies ($\Delta E^{\ddagger}_{dist}$), interaction energies ($\Delta E^{\ddagger}_{int}$), overall electronic energies of activation ($\Delta E^{\ddagger}$), and free energies of activation ($\Delta G^{\ddagger}$). $\Delta E^{\ddagger}_{dist}$, $\Delta E^{\ddagger}_{int}$, and $\Delta E^{\ddagger}$ denoted here are calculated using the single-point energies obtained with M06-2X,[24] the polarized, triple-ζ valence quality def2-TZVPP basis set of Weigend and Ahlrichs,[25] and an ultrafine integration grid within the CPCM model (methanol).

In order to further explain the relative reactivities observed with substituted Sondheimer dialkynes, we applied the distortion/interaction (D/I) model developed by Ess and Houk co-workers to selected substrates.[30,31] This model deconstructs the activation energy $\Delta E^{\ddagger}_{act}$ into distortion energy $\Delta E^{\ddagger}_{dist}$ and interaction energy $\Delta E^{\ddagger}_{int}$ (Figure 6a). Distortion energy is the energy needed to distort the starting alkyne and azide to transform them into their preferred transition-state geometries, whereas the interaction energy is the energy released upon favorable orbital interactions between these distorted reactants. This model has previously been applied to various SPAAC reaction systems, and it has been generally observed that steric effects induced by the presence of a substituent are reflected in an increased distortion energy, whereas the interaction energy encompasses the electronic effects introduced by the substituent.[20,23,32] Hence, we used this model to calculate the distortion ($\Delta E^{\ddagger}_{dist}$) and interaction energies ($\Delta E^{\ddagger}_{int}$) for our reaction in order to investigate the steric and electronic effects of different substituents on Sondheimer dialkyne SPAAC reactivity.

https://dx.doi.org/10.1021/acsomega.9b03459
ACS Omega 2020, 5, 1157−1169

The results from D/I analysis (Figure 6b) demonstrated that the presence of an ortho-substituent next to the alkyne has a significant effect on the distortion energy. For instance, installation of an *ortho*-fluoro (**12**) caused an increase in the distortion energy $\Delta E^{\ddagger}_{dist}$ (by 1.3 kcal/mol) and a slight increase in the interaction energy $\Delta E^{\ddagger}_{int}$ (by 0.4 kcal/mol), leading to an overall increase in the activation energy $\Delta E^{\ddagger}$ (by 0.9 kcal/mol). The most significant effect was observed with the bulkier dimethylamine substituent at the ortho-position (**30**), which led to a considerable increase in the distortion energy $\Delta E^{\ddagger}_{dist}$ (by 1.8 kcal/mol) and no change in the interaction energy, leading to an even higher overall activation barrier $\Delta E^{\ddagger}$ (by 1.8 kcal/mol). This clearly reflects the steric hindrance offered to the SPAAC reaction in the presence of an ortho-substituent which becomes more significant in the presence of an even bulkier substituent, overall resulting in an observed sluggish reactivity of these dialkynes. This is also in accordance with the D/I analysis results shown previously with BARAC in the presence of an *ortho*-fluoro/methyl substituent.[20] On the other hand, installation of a substituent at the meta-position of Sondheimer dialkyne (**11** and **27**) did not have a considerable effect on the D/I energetics.

CONCLUSIONS

In conclusion, we have reported the synthesis of substituted variants of the Sondheimer dialkyne and their application in the double strain-promoted stapling of a p53-based diazido peptide **2** to generate four novel functionalized stapled peptide inhibitors of the oncogenic p53-MDM2 PPI. Minor changes in the aromatic substitution pattern around the aromatic rings of the stapled peptides were found to affect both MDM2 binding affinity and p53 cellular activity. The fluoro-functionalized stapled peptide **22** was found to be the most potent inhibitor in a p53-reporter cell-based assay. Overall, this study demonstrates that substituted Sondheimer dialkynes can be employed in double strain-promoted stapling as a means to readily access functionally diverse stapled peptides. In the future, this approach could conceivably be used to develop potent functionalized stapled peptide inhibitors of other therapeutically relevant PPIs. Reactivity investigations, through experimental studies and density functional theory calculations, suggested the involvement of steric and electronic effects induced by the substituent in determining the reactivity of the substituted Sondheimer dialkyne.

EXPERIMENTAL SECTION

General. *Solvents and Reagents.* Tetrahydrofuran was dried over sodium wire and distilled from a mixture of calcium hydride and lithium aluminium hydride with triphenylmethane as the indicator. Diethyl ether was distilled from a mixture of calcium hydride and lithium aluminium hydride. Dichloromethane, methanol, hexane, acetonitrile, and toluene were distilled from calcium hydride. Petroleum ether refers to the fraction of petroleum ether boiling in the range 40−60 °C. All other reagents and solvents were used as supplied, without prior purification.

Chromatography. Flash column chromatography was carried out using Kieselgel 60 silica (230−400 mesh) with distilled solvents under a positive pressure of nitrogen. Thin-layer chromatography was carried out on glass Merck Kieselgel 60 F254 plates, visualized by ultraviolet irradiation (254 and 365 nm)

NMR Spectroscopy. NMR spectra were recorded on a Bruker Ultrashield 500 (^{1}H: 500 MHz and ^{13}C: 126 MHz) spectrometer. Chemical shifts are quoted in ppm and are referenced to the residual nondeuterated solvent peak and are reported based on the appearance rather than interpretation. ^{1}H spectra are reported as follows: δ_H (spectrometer frequency, solvent): ppm (no. of protons, multiplicity, *J*-coupling constant(s), assignment). ^{13}C spectra are reported as follows: δ_C (spectrometer frequency, solvent): ppm (assignment). Spectral assignment was aided by the results of DEPT, COSY, HMBC, and HSQC experiments where appropriate.

IR Spectroscopy. IR spectra were recorded neat on a PerkinElmer Spectrum One FT-IR spectrophotometer fitted with an attenuated total reflectance sampling accessory. Absorption maxima are reported in wavenumbers (cm^{-1}).

High Resolution Mass Spectrometry. Accurate masses were recorded on a Waters LCT Premier Time of Flight mass spectrometer or Micromass Quadrupole-Time of Flight mass spectrometer. Reported mass values are within the error limits of ±5 ppm.

Liquid Chromatography−Mass Spectrometry. Liquid chromatography−mass spectrometry chromatographs were obtained on an Agilent 1200 series LC using a Supelcosil ABZ + PLUS column (33 mm × 4.6 mm, 3 μm), together with an ESCi Multi-Mode Ionisation Waters ZQ spectrometer using MassLynx 4.1 software. Chromatographs were monitored by absorbance using diode array detection at a wavelength range of 190−600 nm.

High-Performance Liquid Chromatography. Analytical high-performance liquid chromatography (HPLC) chromatographs were obtained on an Agilent 1260 Infinity, eluting with a gradient of 5−40% MeCN (with 0.05% TFA) in water (with 0.1% TFA) over 15 min. Semi-preparative HPLC was run on an Agilent 1260 Infinity, eluting with a gradient of 5−65% MeCN (with 0.05% TFA) in water (with 0.1% TFA) over 20 min. Retention times are reported to the nearest 0.01 min.

Melting Points. All melting points were measured on a Büchi B545 melting point apparatus and are uncorrected. Solvents are reported in parentheses where solids were purified by recrystallization.

Naming and Numbering of Compounds. Where given, systematic compound names are those generated by ChemBioDraw Ultra 13.0 following IUPAC conventions. The numbering of atoms for spectral assignment purposes is arbitrary and not necessarily consistent with the IUPAC name.

Synthetic Procedures. *Methyl 4-Fluoro-2-((phenylsulfonyl)methyl)benzoate* ***16.*** To a suspension of methyl 4-fluoro-2-methylbenzoate **15** (2.0 g, 11.89 mmol) in CCl_4 (59 mL) at 80 °C under N_2 were added NBS (2.23 g, 12.49 mmol) and AIBN (0.19 g, 1.19 mmol), and then the resulting mixture was heated at 100 °C. After stirring at this temperature for 6 h, the reaction mixture was cooled to rt. The reaction mixture was diluted with saturated aqueous NH_4Cl (60 mL) and extracted with CH_2Cl_2 (3 × 60 mL). The organic layers were combined, dried ($MgSO_4$), filtered, and concentrated in vacuo. To the resulting crude product (3.23 g, 13.07 mmol) were added benzenesulfinic acid sodium salt dihydrate (2.58 g, 15.71 mmol) and DMF (20 mL). After the resulting mixture had been stirred at 80 °C overnight, it was cooled to rt. The reaction mixture was diluted with water (40 mL) and extracted with EtOAc (3 × 40 mL). The organic layers were combined, dried ($MgSO_4$), filtered, and concentrated in vacuo. Purification via flash column

https://dx.doi.org/10.1021/acsomega.9b03459
ACS Omega 2020, 5, 1157−1169

chromatography on silica gel (PE/Et_2O = 2:1) gave **16** (2.57 g, 70%) as a white solid.

mp 122−124 °C. ν_{max} (neat): 2954 (C−H), 1717 (C═O), 1589, 1306 (S═O), 1273, 1252, 1151 (S═O), 1117. δ_H (500 MHz, $CDCl_3$): 7.93 (1H, dd, *J* 8.52, 5.81, Ar H), 7.71−7.65 (2H, m, Ar H), 7.62 (1H, t, *J* 7.47, Ar H), 7.52−7.43 (2H, m, Ar H), 7.14−7.04 (2H, m, Ar H), 5.04 (2H, s, H6), 3.74 (3H, s, H11). δ_C (126 MHz, $CDCl_3$): 166.1 (C12), 164.2 (d, *J* 255.14, C3), 138.2 (Ar C), 133.7 (Ar CH), 133.5 (d, *J* 9.02, Ar CH), 132.4 (d, *J* 8.76, Ar CH), 128.9 (Ar CH), 128.6 (Ar CH), 126.8 (Ar C), 120.4 (d, *J* 22.68, Ar CH), 115.9 (d, *J* 21.14, Ar CH), 58.9 (C6), 52.2 (C11). δ_F (376 MHz, $CDCl_3$): −105.7. HRMS (ES^+): found 309.0584; $C_{15}H_{14}O_4F^{32}S$ $[M + H]^+$, requires 309.0597.

(4-Fluoro-2-((phenylsulfonyl)methyl)phenyl)methanol ***17***. To a solution of **16** (2.48 g, 8.04 mmol) in CH_2Cl_2 (24.1 mL) was added DIBAL-H (1.0 M in hexane, 18.5 mL, 18.5 mmol) at −78 °C. After the mixture had been stirred at this temperature for 2 h, saturated aqueous NH_4Cl (100 mL) was poured into the mixture followed by 1 M HCl (100 mL). The product was then extracted with CH_2Cl_2 (3 × 200 mL). The organic layers were combined, dried ($MgSO_4$), filtered, and concentrated in vacuo to afford the pure product **17** as a white solid (2.04 g, 90%).

mp 145−149 °C. ν_{max} (neat): 3479 (O−H), 1592, 1499, 1447, 1305 (S═O), 1146 (S═O), 1081. δ_H (500 MHz, $CDCl_3$): 7.80−7.74 (2H, m, Ar H), 7.69 (1H, t, *J* 7.69, Ar H), 7.59−7.51 (2H, m, Ar H), 7.41 (1H, dd, *J* 8.49, 5.77, H1), 7.05 (1H, td, *J* 8.29, 2.67, H2), 6.68 (1H, dd, *J* 9.17, 2.66, H4), 4.61 (2H, s, H12), 4.50 (2H, s, H6), 2.61 (1H, br s, H11). δ_C (126 MHz, $CDCl_3$): 161.8 (d, *J* 247.68, C3), 137.8 (Ar C), 136.9 (Ar C), 134.3 (Ar CH), 132.2 (d, *J* 8.24, C1), 129.3 (Ar CH), 128.6 (Ar CH), 128.2 (d, *J* 7.97, Ar C), 119.2 (d, *J* 22.66, C4), 116.4 (d, *J* 20.77, C2), 62.5 (C12), 59.4 (C6). δ_F (376 MHz, $CDCl_3$): −113.4. HRMS (ES^+): found 303.0465; $C_{14}H_{13}O_3F^{32}SNa$ $[M + Na]^+$, requires 303.0462.

4-Fluoro-2-((Phenylsulfonyl)methyl)benzaldehyde ***3***. To a solution of **17** (2.08 g, 7.42 mmol) in CH_2Cl_2 (22.0 mL) was added DMP (3.46 g, 8.16 mmol) at rt. After the reaction mixture had been stirred for 3 h, the reaction mixture was diluted with CH_2Cl_2 (15 mL) and poured into saturated $Na_2S_2O_3$ solution (30 mL). The mixture was stirred to dissolve the solid, and the layers were separated. The CH_2Cl_2 layer was then extracted with saturated aqueous $Na_2S_2O_3$ (2 × 30 mL) followed by saturated aqueous $NaHCO_3$ (2 × 30 mL). CH_2Cl_2 was then removed in vacuo, and purification via flash column chromatography on silica gel (EtOAc/hexane = 1:2) gave pure product **3** (1.3 g, 63%) as a white solid.

mp 138−140 °C. ν_{max} (neat): 2988, 1693 (C═O), 1585, 1447, 1306 (S═O), 1238, 1150 (S═O), 1083. δ_H (400 MHz, $CDCl_3$): 9.81 (1H, s, H11), 7.82−7.72 (3H, m, Ar H), 7.65 (1H, t, *J* 7.48, Ar H), 7.54−7.46 (2H, m, Ar H), 7.32−7.18 (2H, m, Ar H), 5.04 (2H, s, H6). δ_C (126 MHz, $CDCl_3$): 190.4 (C11), 165.0 (d, *J* 258.44, C3), 138.1 (Ar C), 137.1 (d, *J* 9.92, Ar CH), 134.1 (Ar CH), 132.2 (d, *J* 9.39, Ar C), 131.3 (d, *J* 3.08, Ar C), 129.0 (Ar CH), 128.6 (Ar CH), 121.1 (d, *J* 22.97, C4), 116.6 (d, *J* 21.60, Ar CH), 57.2 (C6). δ_F (376 MHz, $CDCl_3$): −102.3. HRMS (ES^+): found 279.0489; $C_{14}H_{12}O_3{}^{32}SF$ $[M + H]^+$, requires 279.0491.

(5E,11E)-2,8-Difluoro-6,12-bis(phenylsulfonyl)dibenzo-[a,e][8]annulene ***7***. A mixture of **3** (0.80 g, 2.88 mmol) and $ClP(O)(OEt)_2$ (0.5 mL, 3.46 mmol) in THF (58 mL) was cooled to −78 °C, and then LiHMDS (1.0 M in THF, 5.8 mL, 5.8 mmol) was added. After stirring at −78 °C for 30 min, the reaction mixture was warmed to rt and stirred for a further 1.5 h. Saturated aqueous NH_4Cl (8 mL) was poured into the mixture. The reaction mixture was diluted with water (90 mL) and extracted with EtOAc (3 × 100 mL). The organic layers were combined, dried ($MgSO_4$), filtered, and concentrated in vacuo. Purification via flash column chromatography on silica gel (EtOAc/hexane = 3:8) gave **7** as a pale yellow solid (0.28 g, 19%).

mp 203 °C (dec.). ν_{max} (neat): 2923, 1579, 1493, 1447, 1319 (S═O), 1222, 1151 (S═O), 1084. δ_H (500 MHz, $CDCl_3$): 7.66 (2H, t, *J* 7.19, Ar H), 7.54−7.44 (8H, m, Ar H), 7.33 (2H, s, Ar H), 7.21 (2H, dd, *J* 9.33, 2.50, Ar H), 7.06−6.94 (4H, m, Ar H). δ_C (126 MHz, $CDCl_3$): 162.0 (d, *J* 250.77, C3), 144.4 (Ar C), 138.6 (Ar CH), 136.6 (Ar C), 134.1 (Ar CH), 131.2 (Ar C), 131.1 (d, *J* 8.80, Ar C), 129.1 (Ar CH), 128.9 (d, *J* 8.59, Ar CH), 128.1 (Ar CH), 117.9 (d, *J* 23.49, Ar CH), 117.1 (d, *J* 21.88, Ar CH). δ_F (376 MHz, $CDCl_3$): −110.6. HRMS (ES^+): found 521.0704; $C_{28}H_{19}F_2O_4{}^{32}S_2$ $[M + H]^+$, requires 521.0693.

2,8-Difluoro-5,6,11,12-tetradehydrodibenzo[a,e]-cyclooctene ***11***. A solution of **7** (0.11 g, 0.21 mmol) in THF (5.3 mL) was cooled to −78 °C, and then LDA (1.0 M in THF/hexane, 0.85 mL, 0.85 mmol) was added. The reaction mixture was stirred at this temperature for 2 h, and saturated aqueous NH_4Cl (9 mL) was poured into the mixture. The reaction mixture was cooled to rt, diluted with water (25 mL), and extracted with CH_2Cl_2 (3 × 35 mL). The organic layers were combined, dried ($MgSO_4$), filtered, and concentrated in vacuo. Purification via flash column chromatography on silica gel (EtOAc/hexane = 1:8) gave **11** as a yellow solid (15 mg, 30%).

ν_{max} (neat): 2922, 1569, 1461, 1243, 977, 778. δ_H (500 MHz, $CDCl_3$): 6.98−6.91 (2H, m, Ar H), 6.73 (2H, t, *J* 8.74, Ar H), 6.59 (2H, d, Ar H). δ_C (126 MHz, $CDCl_3$): 158.6 (d, *J* 254.49, C3), 134.3 (Ar C), 131.0 (d, *J* 8.54, Ar CH), 123.2 (d, *J* 2.93, Ar CH), 119.8 (d, *J* 16.54, Ar C), 117.8 (d, *J* 21.06, Ar CH), 111.4 (C≡C), 104.9 (C≡C). δ_F (376 MHz, $CDCl_3$): −107.7. HRMS (ES^+): found 236.0428; $C_{16}H_6F_2$ $[M + H]^+$, requires 236.0438.

3-Fluoro-2-((phenylsulfonyl)methyl)benzonitrile ***20***. To a suspension of 3-fluoro-2-methylbenzonitrile **18** (5.28 g, 39.1 mmol) in CCl_4 (196.0 mL) at 80 °C under N_2 were added NBS (7.31 g, 41.06 mmol) and AIBN (0.64 g, 3.91 mmol), and then the resulting mixture was heated at 100 °C. After stirring at this temperature for 6 h, the reaction mixture was cooled to rt. The reaction mixture was diluted with saturated aqueous NH_4Cl (150 mL) and extracted with CH_2Cl_2 (3 × 150 mL). The organic layers were combined, dried ($MgSO_4$), filtered, and concentrated in vacuo. To the resulting crude product (8.63 g, 40.33 mmol) were added benzenesulfinic acid sodium salt dihydrate (7.94 g, 48.4 mmol) and DMF (60.5 mL). After the resulting mixture had been stirred at 80 °C overnight, it was cooled to rt. The reaction mixture was diluted with water (100 mL) and extracted with EtOAc (3 × 100 mL). The organic layers were combined, dried ($MgSO_4$), filtered, and concentrated in vacuo. Purification via flash column chromatography on silica gel (PE/Et_2O = 2:1) gave **20** (6.56 g, 61%) as a white solid.

mp 156−158 °C. ν_{max} (neat): 2236 (C≡N), 1575, 1321 (S═O), 1253, 1137 (S═O), 1084. δ_H (500 MHz, $CDCl_3$): 7.84−7.78 (2H, m, Ar H), 7.70 (1H, t, *J* 7.49, Ar H), 7.59−7.52 (2H, m, Ar H), 7.51−7.45 (2H, m, Ar H), 7.39−7.31 (1H, m, Ar H), 4.63 (2H, s, H6). δ_C (126 MHz, $CDCl_3$): 161.4 (d, *J* 254.59, C4), 138.0 (Ar C), 134.5 (Ar CH), 131.5 (d, *J* 8.98, Ar CH), 129.4 (Ar CH), 129.1 (d, *J* 3.85, Ar CH), 128.7 (Ar CH), 120.7 (d, *J* 22.15, Ar CH), 119.7 (d, *J* 17.48, Ar C), 116.3 (CN), 115.6

https://dx.doi.org/10.1021/acsomega.9b03459
ACS Omega 2020, 5, 1157−1169

(Ar C), 55.0 (C6). δ_F (376 MHz, $CDCl_3$): −109.8. HRMS (ES^+): found 276.0498; $C_{14}H_{11}NO_2{}^{32}SF$ $[M + H]^+$, requires 276.0495.

(5E,11E)-1,7-Difluoro-6,12-bis(phenylsulfonyl)dibenzo-[a,e][8]annulene ***8***. To a solution of **20** (1.06 g, 3.88 mmol) in CH_2Cl_2 (19.4 mL) was added DIBAL-H (1.0 M in hexane, 7.77 mL, 7.77 mmol) at −78 °C. After the mixture had been stirred at this temperature for 2 h, saturated aqueous NH_4Cl (50 mL) was poured into the mixture followed by 1 M HCl (50 mL). The product was then extracted with CH_2Cl_2 (3 × 100 mL). The organic layers were combined, dried ($MgSO_4$), filtered, and concentrated in vacuo. Purification via flash column chromatography on silica gel (EtOAc/hexane = 1:2) gave **4** (0.70 g, 65%) as a crude white solid consisting of an inseparable mixture of the desired aldehyde product (major) and the starting material. A mixture of crude **4** (0.52 g, 1.85 mmol) and ClP(O)$(OEt)_2$ (0.32 mL, 2.23 mmol) in THF (37 mL) was cooled to −78 °C, and then LiHMDS (1.0 M in THF, 3.71 mL, 3.71 mmol) was added. After stirring at −78 °C for 30 min, the reaction mixture was warmed to rt and stirred for a further 1.5 h. Saturated aqueous NH_4Cl (5 mL) was poured into the mixture. The reaction mixture was diluted with water (50 mL) and extracted with EtOAc (3 × 60 mL). The organic layers were combined, dried ($MgSO_4$), filtered, and concentrated in vacuo. Purification via flash column chromatography on silica gel (EtOAc/hexane = 3:8) gave **8** as a pale yellow solid (0.22 g, 23%).

mp 190−193 °C. ν_{max} (neat): 1571, 1446, 1319 (S═O), 1260, 1146 (S═O), 1085. δ_H (500 MHz, $CDCl_3$): 7.67 (2H, t, *J* 7.11), 7.57−7.46 (10H, m, Ar H), 7.33−7.27 (2H, m, Ar H), 6.95−6.86 (4H, m, Ar H). δ_C (126 MHz, $CDCl_3$): 160.2 (d, *J* 253.97, C4), 142.7 (Ar C), 140.6 (Ar CH), 138.5 (Ar C), 138.0 (Ar C), 134.0 (Ar CH), 131.5 (d, *J* 8.80, Ar CH), 129.2 (Ar CH), 128.6 (Ar CH), 122.6 (Ar CH), 117.4 (d, *J* 17.06, Ar C), 116.3 (d, *J* 21.80, Ar CH). δ_F (376 MHz, $CDCl_3$): −105.5. HRMS (ES^+): found 521.0693; $C_{28}H_{19}O_4{}^{32}S_2F_2$ $[M + H]^+$, requires 521.0693.

1,7-Difluoro-5,6,11,12-tetradehydrodibenzo[a,e]-cyclooctene ***12***. A solution of **8** (0.13 g, 0.24 mmol) in THF (4.9 mL) was cooled to −78 °C, and then LDA (1.0 M in THF/hexane, 0.98 mL, 0.98 mmol) was added. The reaction mixture was stirred at this temperature for 2 h, and saturated aqueous NH_4Cl (7 mL) was poured into the mixture. The reaction mixture was cooled to rt, diluted with water (20 mL), and extracted with CH_2Cl_2 (3 × 30 mL). The organic layers were combined, dried ($MgSO_4$), filtered, and concentrated in vacuo. Purification via flash column chromatography on silica gel (EtOAc/hexane = 1:8) gave **12** as a yellow solid (15 mg, 26%).

mp 140 °C (dec.). ν_{max} (neat): 2156 (C≡C), 1574, 1448, 1181, 877, 815. δ_H (500 MHz, $CDCl_3$): 6.74−6.68 (2H, m, Ar H), 6.62 (2H, td, *J* 8.41, 2.61, Ar H), 6.48 (2H, dd, *J* 8.70, 2.60, Ar H). δ_C (126 MHz, $CDCl_3$): 163.0 (d, *J* 250.97, C4), 135.3 (d, *J* 10.12), 128.2 (d, *J* 8.78, Ar CH), 115.22 (Ar CH), 115.23 (d, *J* 45.55, Ar C), 109.9 (C≡C), 107.4 (C≡C). δ_F (376 MHz, $CDCl_3$): −109.5. HRMS (ES^+): found 236.0427; $C_{16}H_6F_2$ $[M + H]^+$, requires 236.0438.

4-Methoxy-2-((phenylsulfonyl)methyl)benzonitrile ***21***. To a suspension of 4-methoxy-2-methylbenzonitrile **19** (4.00 g, 27.21 mmol) in CCl_4 (80.0 mL) at 80 °C under N_2 were added NBS (5.81 g, 32.65 mmol) and benzoyl peroxide (329 mg, 1.36 mmol), and then the resulting mixture was heated at 80 °C. After stirring at this temperature for 6 h, the reaction mixture was cooled to rt. The reaction mixture was diluted with saturated aqueous NH_4Cl (80 mL) and extracted with CH_2Cl_2 (3 × 80 mL). The organic layers were combined, dried ($MgSO_4$), filtered, and concentrated in vacuo. To the resulting crude product were added benzenesulfinic acid sodium salt dihydrate (6.69 g, 40.82 mmol) and DMF (80.0 mL). After the resulting mixture had been stirred at 80 °C overnight, it was cooled to rt. The reaction mixture was diluted with water (100 mL) and extracted with EtOAc (3 × 100 mL). The organic layers were combined, dried ($MgSO_4$), filtered, and concentrated in vacuo. Purification via flash column chromatography on silica gel (EtOAC/hexane = 1:2) gave **21** (6.24 g, 81%) as a white solid.

mp 144−145 °C. ν_{max} (neat): 2944, 2221 (C≡N), 1609, 1499, 1291 (S═O), 1147 (S═O), 1082, 1025. δ_H (500 MHz, $CDCl_3$): 7.73 (2H, dd, *J* 8.4, 1.2, H8), 7.69−7.62 (1H, m, H10), 7.53−7.47 (2H, m, H9), 7.44 (1H, d, *J* 8.7, H1), 7.10 (1H, d, *J* 2.5, H4), 6.93 (1H, dd, *J* 8.7, 2.5, H2), 4.52 (2H, s, H6), 3.87 (3H, s, H13). δ_C (126 MHz, $CDCl_3$): 162.8 (C3), 137.7 (C7), 134.4 (Ar CH), 134.4 (Ar CH), 133.8 (C12), 129.4 (C9), 128.8 (C8), 117.4 (C4), 117.1 (C11), 115.7 (C2), 106.0 (C5), 60.7 (C6), 55.9 (C13). HRMS (ES^+): found 288.0686; $C_{15}H_{14}NO_3{}^{32}S$ $[M + H]^+$, requires 288.0689. Characterization data is in accordance with that previously reported.[33]

4-Methoxy-2-((phenylsulfonyl)methyl)benzaldehyde ***5***. To a solution of **21** (1.0 g, 3.48 mmol) in CH_2Cl_2 (10.0 mL) was added DIBAL-H (1.0 M in hexane, 5.22 mL, 5.22 mmol) at −78 °C. After the mixture had been stirred at this temperature for 2 h, saturated aqueous NH_4Cl (25 mL) was poured into the mixture, followed by 1 M HCl (25 mL). The product was then extracted with CH_2Cl_2 (3 × 50 mL). The organic layers were combined, dried ($MgSO_4$), filtered, and concentrated in vacuo. Purification via flash column chromatography on silica gel (EtOAc/hexane = 1:2) gave **5** (0.60 g, 59%) as a white solid.

δ_H (500 MHz, $CDCl_3$): 9.65 (1H, s, H11), 7.73−7.70 (2H, m, H8), 7.63 (1H, d, *J* 8.5, H1), 7.62−7.57 (1H, m, H10), 7.48−7.42 (2H, m, H9), 7.01 (1H, dd, *J* 8.5, 2.5, H2), 6.97 (1H, d, *J* 2.5, H4), 5.04 (2H, s, H6), 3.88 (3H, s, H13). δ_C (126 MHz, $CDCl_3$): 190.8 (C11), 163.4 (C3), 138.5 (C7), 137.4 (C1), 133.9 (C10), 131.4 (C12), 128.9 (C9), 128.8 (C8), 128.1 (C5), 119.5 (C4), 114.6 (C2), 57.7 (C6), 55.9 (C13). HRMS (ES^+): found 291.0683; $C_{15}H_{15}O_4{}^{32}S$ $[M + H]^+$, requires 291.0686. Characterization data is in accordance with that previously reported.[34]

2,8-Dimethoxy-5,6,11,12-tetradehydrodibenzo[a,e]-cyclooctene ***13***. A mixture of **5** (0.50 g, 1.72 mmol) and ClP(O)$(OEt)_2$ (0.30 mL, 2.07 mmol) in THF (35.0 mL) was cooled to −78 °C, and then LiHMDS (1.0 M in THF, 3.79 mL, 3.79 mmol) was added. After stirring at −78 °C for 30 min, the reaction mixture was warmed to rt and stirred for a further 1.5 h. LDA (1.0 M in THF/hexane, 8.62 mL, 8.62 mmol) was then added at −78 °C, and the reaction mixture was stirred at this temperature for 2 h, and saturated aqueous NH_4Cl (13.0 mL) was poured into the mixture. The reaction mixture was diluted with water (26.0 mL) and extracted with EtOAc (3 × 40 mL). The organic layers were combined, dried ($MgSO_4$), filtered, and concentrated in vacuo. Purification via flash column chromatography on silica gel (EtOAc/hexane = 1:3) gave **13** as a yellow solid (88 mg, 39%).

mp 171−173 (dec) °C. ν_{max} (neat): 2916, 2849, 2145, 1595, 1562, 1421, 1318, 1213, 1065, 1024. δ_H (500 MHz, $CDCl_3$): 6.67 (2H, d, *J* 8.4, Ar H), 6.39 (2H, dd, *J* 8.4, 2.6, Ar H), 6.34 (2H, d, *J* 2.6, Ar H), 3.72 (6H, s, H9). δ_C (126 MHz, $CDCl_3$): 160.4 (C3), 135.0, 128.0 (C1), 124.0 (C8), 114.7 (C4), 112.0 (C2), 110.3 (C≡C), 107.4 (C≡C), 55.5 (C9). HRMS (ES^+): found 261.0904; $C_{18}H_{13}O_2$ $[M + H]^+$, requires 261.0910.

https://dx.doi.org/10.1021/acsomega.9b03459
ACS Omega 2020, 5, 1157−1169

1,2-Dimethoxy-4-methyl-5-((phenylsulfonyl)methyl)-benzene ***33***. A suspension of 3,4-dimethoxytoluene (1.52 g, 10.0 mmol) and paraformaldehyde (0.45 g, 15.0 mmol) in dry CCl_4 (16.6 mL) was cooled to 0 °C under N_2. To this suspension a solution of HBr/AcOH (33%, 4.0 mL) was added dropwise over 3−5 min, and the resulting mixture was stirred for 4 h at 0 °C. The reaction mixture was poured into cold water (33.3 mL), and the organic layer was separated, washed with 5% $NaHCO_3$(aq), and dried over anhydrous $MgSO_4$. Evaporation of the solvents in vacuo afforded a white solid. To this crude product, benzenesulfinic acid sodium salt dihydrate (2.40 g, 12.0 mmol) and DMF (16.6 mL) were added. After stirring at 80 °C overnight, the reaction mixture was cooled to rt. The reaction mixture was diluted with water (30 mL) and extracted with EtOAc (3 × 50 mL). The organic layers were combined, dried ($MgSO_4$), filtered, and concentrated in vacuo. Purification via flash column chromatography on silica gel (EtOAc/hexane = 1:8) gave **33** (2.63 g, 86%) as a white solid.

mp 158−160 °C. δ_H (500 MHz, $CDCl_3$): 7.71−7.60 (3H, m, H9, 11), 7.54−7.45 (2H, m, H10), 6.61 (1H, s, H14), 6.44 (1H, s, H5), 4.31 (2H, s, H7), 3.86 (3H, s, H3), 3.68 (3H, s, H1), 2.05 (3H, s, H12). δ_C (126 MHz, $CDCl_3$): 149.1 (C4), 146.8 (C2), 138.3 (C8), 133.7 (Ar CH), 131.0 (C6), 128.9 (Ar CH), 128.8 (Ar CH), 118.0 (C13), 114.4 (C5), 113.3 (C14), 59.9 (C7), 55.8 (C1, C3), 18.9 (C12). Characterization data is in accordance with that previously reported.[15]

4,5-Dimethoxy-2-((phenylsulfonyl)methyl)benzaldehyde ***6***. To a suspension of **33** (1.22 g, 4.00 mmol) in CCl_4 (37.0 mL) at 80 °C under N_2 were added NBS (0.75 g, 4.20 mmol) and BPO (97.0 mg, 0.40 mmol), and then the resulting mixture was heated at 100 °C. After stirring at this temperature for 6 h, the reaction mixture was cooled to rt. After workup with CH_2Cl_2/NH_4Cl(aq), the combined organic layers were dried over $MgSO_4$ and evaporated in vacuo. To the resulting crude product were added $CaCO_3$ (4.0 g, 40.0 mmol), dimethoxyethane (13.3 mL), and H_2O (13.3 mL). After the resulting mixture had been heated at 120 °C overnight, it was cooled to rt, and the remaining $CaCO_3$ was neutralized with dilute HCl (aq) solution. The reaction mixture was diluted with water (12 mL) and extracted with CH_2Cl_2 (3 × 20 mL). The organic layers were combined, dried ($MgSO_4$), filtered, and concentrated in vacuo. To this crude product were added MnO_2 (3.48 g, 40.0 mmol) and CH_2Cl_2 (13.3 mL). After the resulting mixture was heated to 50 °C overnight, it was cooled to rt and filtered, and the filtrate was concentrated in vacuo. Purification via flash column chromatography on silica gel (EtOAc/hexane = 1:1) gave **6** as a pale-yellow solid (0.64 g, 50%).

mp 145−147 °C. δ_H (500 MHz, $CDCl_3$): 9.76 (1H, s, H12), 7.71 (2H, dd, *J* 8.43, 1.18, Ar H), 7.66−7.61 (1H, m, Ar H), 7.51−7.46 (2H, m, Ar H), 7.26 (1H, s, H14), 6.80 (1H, s, H5), 4.92 (2H, s, H7), 3.96 (3H, s, H1), 3.91 (3H, s, H3). δ_C (126 MHz, $CDCl_3$): 189.5 (C12), 153.0 (C2), 149.5 (C4), 137.9 (C8), 133.9 (Ar CH), 129.0 (Ar CH), 128.7 (Ar CH), 128.0 (C6), 123.7 (C13), 115.5 (C5), 114.1 (C14), 57.3 (C7), 56.3 (C3), 56.1 (C1). Characterization data is in accordance with that previously reported.[15]

2,3,8,9-Tetramethoxy-5,6,11,12-tetradehydrodibenzo-[a,e]cyclooctene ***14***. A mixture of **6** (185 mg, 0.58 mmol) and $ClP(O)(OEt)_2$ (0.10 mL, 0.69 mmol) in THF (11.5 mL) was cooled to −78 °C, and then LiHMDS (1.0 M in THF, 1.15 mL, 1.15 mmol) was added. After stirring at −78 °C for 30 min, the reaction mixture was warmed to rt and stirred for a further 1.5 h. LDA (1.0 M in THF/hexane, 2.88 mL, 2.88 mmol) was then added at −78 °C, and the reaction mixture was stirred at this temperature for 2 h, and saturated aqueous NH_4Cl (3 mL) was poured into the mixture. The reaction mixture was diluted with water (6 mL) and extracted with EtOAc (3 × 10 mL). The organic layers were combined, dried ($MgSO_4$), filtered, and concentrated in vacuo. Purification via flash column chromatography on silica gel (PE/EtOAc = 1:1) gave **14** as a yellow solid (41 mg, 22%).

mp 205 °C (dec.). δ_H (400 MHz, $CDCl_3$): 6.26 (4H, s, H3), 3.78 (12 H, s, H1). δ_C (101 MHz, $CDCl_3$): 149.0 (C2), 126.2 (C4), 111.4 (C3), 108.9 (C5), 56.2 (C1). Characterization data is in accordance with that previously reported.[15]

Peptide Synthesis Procedure. Peptide synthesis was carried out on solid-phase using an Fmoc-protecting group strategy on a CEM Liberty Automated Microwave Peptide Synthesizer. Merck Rink Amide MBHA resin LL (0.29−0.39 mmol/g) was used. Peptide couplings were conducted with Fmoc-protected amino acids (5 equiv) in DMF, HATU, or HBTU (5 equiv) in DMF as the coupling reagent, and *N*,*N*-diisopropylethylamine (10 equiv) in NMP as the base. Double coupling was used for arginine for 15 min each without microwave irradiation. Single coupling was used for all other amino acids, with 25 W power at 75 °C over 15 min. Fmoc deprotection was carried out using 20% piperidine in DMF, with 45 W power at 75 °C over 3 min. N-terminal capping was carried out manually by treating the resin-bound peptide with acetic anhydride (10 equiv) and *N*,*N*-diisopropylethylamine (10 equiv) in dichloromethane for 45 min. Cleavage was carried out with a cocktail of 95% trifluoroacetic acid, 2.5% water, and 2.5% triisopropylsilane for 2 h. The cleavage solution was then evaporated under a stream of nitrogen and triturated with diethyl ether prior to purification by preparative HPLC. Peptide yields were estimated based on absorbance in the HPLC chromatograph at 220 nm. The concentration of peptides in stock solutions was determined by amino acid analysis at the Peptide Nucleic Acid Chemistry Facility at the Department of Biochemistry, University of Cambridge.

General Strain-Promoted Double-Click Peptide Stapling Procedure. A solution of diazido PDI-E peptide (1 equiv) and dialkyne (1.1 equiv) in 1:1 *t*-BuOH/H_2O (1 mL/mg peptide) was stirred at rt for 16 h. The reaction mixture was lyophilized and purified by HPLC to give the stapled peptide.

Competitive Fluorescence Polarization Assay. Competitive fluorescence polarization (FP) assays were performed as previously described[2,7] in 384-well microplates (Corning) on a CLARIOstar microplate reader (BMG labtech) using an excitation filter 540−20 nm, dichroic mirror LP 566 nm, and emission filter 590−20 nm. All peptides were dissolved in DMSO as stock solutions. The stock concentration of the TAMRA-labeled tracer (TAMRA-RFMDYWEGL-NH_2) was determined based on the 5-TAMRA absorbance at 556 nm (extinction coefficient ε = 89,000 M^{-1} cm^{-1}) measured on a NanoDrop 2000 (Thermo Scientific), and the concentrations of all peptides were determined by amino acid analysis (Department of Biochemistry, University of Cambridge). K_d of the TAMRA-labeled tracer was obtained from previously reported experiments.[2] For the competitive fluorescence polarization assay, the TAMRA-labeled tracer (50 nM) was incubated with MDM2 (95 nM) in PBS buffer containing 0.05% (v/v) Tween 20 at 25 °C for 1 h. The unlabeled peptides or positive controls (nutlin) were diluted twofold serially in PBS buffer containing 0.05% (v/v) Tween 20 for a 16-point titration curve (20 μL per well). To each well containing the unlabeled compound was

https://dx.doi.org/10.1021/acsomega.9b03459
ACS Omega 2020, 5, 1157−1169

added the TAMRA-labeled tracer/MDM2 solution (20 μL), and the mixture was incubated for 1 h at 25 °C before the measurement was taken. Titrations were performed in triplicate. Data were fitted in GraphPad Prism 5.0 using the equations as described previously.[35]

Cellular p53 Reporter Assay. The basic assay was carried out as previously described in the literature[18,36] and is briefly described as follows. T22 cells stably transfected with a p53-responsive β-galactosidase reporter,[18] kindly provided by Prof. Sir David Lane, were grown in DMEM with 10% fetal bovine serum and penicillin/streptomycin. Cells were seeded for 24 h at 8000 cells per 100 μL well in a 96-well black-walled clear flat-bottom polystyrene plate (Greiner #655090), then treated with the peptide in triplicate for 18 h at 37 °C in DMEM with 10% serum and a final DMSO concentration of 1%. The β-galactosidase activity was quantified using a FluoReporter LacZ/Galactosidase Quantitation kit (Invitrogen). Fluorescence measurements were read on a Tecan Infinite 200 Pro plate reader. The in situ stapling version of the assay was identical to the basic assay conditions in all aspects, except that the cells were treated with a pure unstapled PDI-E peptide (50 μM) and substituted Sondheimer dialkynes (0.5 mM). Control cells were treated with only substituted Sondheimer dialkynes (0.5 mM), only unstapled PDI-E peptide (50 μM), or only 1% DMSO.

Kinetic Analysis. The rate measurement of substituted Sondheimer dialkynes **1**, **11**, and **12** in a double strain-promoted click reaction was performed by monitoring the absorbance of dialkynes in the presence of an excess amount of benzyl azide.[8,15] It has been demonstrated previously with Sondheimer diyne **1** that the first cycloaddition leading to the formation of monoyne intermediate is the rate-determining step of the reaction.[8] All UV measurements were recorded using a Varian Cary 300 UV−visible spectrophotometer. General procedure: to 1.5 mL 2 mM solution of substituted dialkyne in MeOH taken in a quartz cuvette was added 1.5 mL of MeOH solution of benzyl azide in 3 different concentrations (100, 200, and 400 mM; final concentration at 50, 100, and 200 mM, respectively). The consumption of dialkyne was monitored by UV spectroscopy at a wavelength that is characteristic for the absorbance of dialkyne but almost no significant absorption is observed for benzyl azide and products. The experiments were repeated in duplicate for each concentration of azide. The observed absorbance data at the characteristic wavelength were plotted versus time and fitted to a first-order exponential decay curve. The pseudo-first order rate constants (k_0) were determined by least-squares fitting of the data to the following exponential equation ($y = A \times \exp(-k_0 \times x) + y_0$) using Origin, where A and y_0 are constants. The pseudo-first order rate constants determined were plotted versus the concentration of azide and fitted to a straight line by a linear regression method using Microsoft Office Excel 16. The slope of the straight line indicates the second-order rate constant (k) for the first cycloaddition in a double strain-promoted click reaction of dialkyne with benzyl azide, which is the rate-determining step of the reaction.

Computational Analysis. All quantum mechanical calculations were performed with Gaussian 09 Rev D.01. All geometries were optimized using the B3LYP density functional and the 6-31G(d) basis set within the conductor-like polarisable continuum solvation model (CPCM)[37,38] for methanol, using the default integration grid. Vibrational frequencies were computed for all optimized structures to verify that they were either minima (zero imaginary frequencies) or transition states (a single imaginary frequency). Single-point energies E (M06-2X) were calculated using M06-2X,[24] the polarised, triple-ζ valence quality def2-TZVPP basis set of Weigend and Ahlrichs,[25] and an ultrafine integration grid within the CPCM model (methanol). The strain-promoted click reaction of substituted Sondheimer dialkynes with methyl azide was modeled at 298.15 K at 1 atm in methanol. Methyl azide was employed as it is less conformationally flexible than benzyl azide, and the calculations showed that it behaves similarly to benzyl azide in a SPAAC with Sondheimer dialkyne.[20] Transition states were calculated for both *anti*- and *syn*-attack of methyl azide on diynes. Previous computational studies with similar methods provided results in accordance with the experiment.[8,20,29] Computationally obtained structures were illustrated with PyMOL. The Gibbs free energy values were determined by addition of the B3LYP thermal correction to the M06-2X energies.[26] This approach has previously been shown to give reliable results when modeling organic reaction.[27,28]

■ ASSOCIATED CONTENT

Supporting Information

The Supporting Information is available free of charge at https://pubs.acs.org/doi/10.1021/acsomega.9b03459.

Full synthetic details, ^{1}H and ^{13}C NMR spectra, crystallographic data in .cif format, and additional details on computations; and the crystal structure data of **27**, **28**, **29**, and **30** (PDF)

■ AUTHOR INFORMATION

Corresponding Authors

Matthew N. Grayson − *University of Bath, Bath, U.K.*; orcid.org/0000-0003-2116-7929; Email: M.N.Grayson@bath.ac.uk

Yu Heng Lau − *The University of Sydney, Sydney, Australia*; Email: yuheng.lau@sydney.edu.au

Laura S. Itzhaki − *University of Cambridge, Cambridge, U.K.*; orcid.org/0000-0001-6504-2576; Email: lsi10@cam.ac.uk

David R. Spring − *University of Cambridge, Cambridge, U.K.*; orcid.org/0000-0001-7355-2824; Email: spring@ch.cam.ac.uk

Other Authors

Krishna Sharma − *University of Cambridge, Cambridge, U.K.*; orcid.org/0000-0001-5220-5823

Alexander V. Strizhak − *University of Cambridge, Cambridge, U.K.*

Elaine Fowler − *University of Cambridge, Cambridge, U.K.*; orcid.org/0000-0002-6942-646X

Wenshu Xu − *University of Cambridge, Cambridge, U.K.*

Ben Chappell − *University of Cambridge, Cambridge, U.K.*

Hannah F. Sore − *University of Cambridge, Cambridge, U.K.*

Warren R. J. D. Galloway − *University of Cambridge, Cambridge, U.K.*

Complete contact information is available at: https://pubs.acs.org/10.1021/acsomega.9b03459

Notes

The authors declare no competing financial interest.

https://dx.doi.org/10.1021/acsomega.9b03459
ACS Omega 2020, 5, 1157−1169

The crystal structure data of **27**, **28**, **29**, and **30** have been deposited in the Cambridge Crystallographic Data Center (CCDC 1853508-1853511, respectively)

■ ACKNOWLEDGMENTS

D.R.S. acknowledges support from the Engineering and Physical Sciences Research Council (EP/P020291/1) and Royal Society (Wolfson Research Merit Award). K.S. would like to thank Trinity College, Cambridge Trust, Cambridge Nehru Trust and the Cambridge Philosophical Society for providing fellowships. M.N.G. thanks the University of Bath for financial support. B.C. thanks Herchel Smith Trust for funding. We thank Dr. Andrew Bond for X-ray crystallography, Balasubrmanian group (Department of Chemistry, University of Cambridge) for use of their UV spectrometer, and the PNAC service (Department of Biochemistry, University of Cambridge). We would like to thank X-ray crystallographic facility at the Department of Biochemistry for access to crystallisation instrumentation. We are grateful for the Diamond Light Source for access to beamline I04 (proposal mx14043) and for the data that contributed to these results. Part of this work was performed using the Darwin Supercomputer of the University of Cambridge High Performance Computing Service (http://www.hpc.cam.ac.uk/), provided by Dell Inc. using Strategic Research Infrastructure Funding from the Higher Education Funding Council for England and funding from the Science and Technology Facilities Council.

■ REFERENCES

(1) Lau, Y. H.; de Andrade, P.; Wu, Y.; Spring, D. R. Peptide stapling techniques based on different macrocyclisation chemistries. *Chem. Soc. Rev.* **2015**, *44*, 91−102.

(2) Lau, Y. H.; de Andrade, P.; Quah, S.-T.; Rossmann, M.; Laraia, L.; Sköld, N.; Sum, T. J.; Rowling, P. J. E.; Joseph, T. L.; Verma, C.; Hyvönen, M.; Itzhaki, L. S.; Venkitaraman, A. R.; Brown, C. J.; Lane, D. P.; Spring, D. R. Functionalised staple linkages for modulating the cellular activity of stapled peptides. *Chem. Sci.* **2014**, *5*, 1804−1809.

(3) Sharma, K.; Kunciw, D. L.; Xu, W.; Wiedmann, M. M.; Wu, Y.; Sore, H. F.; Galloway, W. R. J. D.; Lau, Y. H.; Itzhaki, L. S.; Spring, D. R. CHAPTER 8 Double-click Stapled Peptides for Inhibiting Protein-Protein Interactions. *Cyclic Peptides: From Bioorganic Synthesis to Applications*; RSC, 2018; pp 164−187.

(4) Walensky, L. D.; Bird, G. H. Hydrocarbon-Stapled Peptides: Principles, Practice, and Progress. *J. Med. Chem.* **2014**, *57*, 6275−6288.

(5) Klein, M. A. Stabilized Helical Peptides: A Strategy to Target Protein−Protein Interactions. *ACS Med. Chem. Lett.* **2014**, *5*, 838−839.

(6) Pelay-Gimeno, M.; Glas, A.; Koch, O.; Grossmann, T. N. Structure-Based Design of Inhibitors of Protein−Protein Interactions: Mimicking Peptide Binding Epitopes. *Angew. Chem., Int. Ed.* **2015**, *54*, 8896−8927.

(7) Lau, Y. H.; Wu, Y.; Rossmann, M.; Tan, B. X.; de Andrade, P.; Tan, Y. S.; Verma, C.; McKenzie, G. J.; Venkitaraman, A. R.; Hyvönen, M.; Spring, D. R. Double Strain-Promoted Macrocyclization for the Rapid Selection of Cell-Active Stapled Peptides. *Angew. Chem., Int. Ed.* **2015**, *54*, 15410−15413.

(8) Kii, I.; Shiraishi, A.; Hiramatsu, T.; Matsushita, T.; Uekusa, H.; Yoshida, S.; Yamamoto, M.; Kudo, A.; Hagiwara, M.; Hosoya, T. Strain-promoted double-click reaction for chemical modification of azido-biomolecules. *Org. Biomol. Chem.* **2010**, *8*, 4051−4055.

(9) Wong, H. N. C.; Garratt, P. J.; Sondheimer, F. Unsaturated eight-membered ring compounds. XI. Synthesis of sym-dibenzo-1,5-cyclo-octadiene-3,7-diyne and sym-dibenzo-1,3,5-cyclooctatrien-7-yne, presumably planar conjugated eight-membered ring compounds. *J. Am. Chem. Soc.* **1974**, *96*, 5604−5605.

(10) Agard, N. J.; Prescher, J. A.; Bertozzi, C. R. A Strain-Promoted [3 + 2] Azide−Alkyne Cycloaddition for Covalent Modification of Biomolecules in Living Systems. *J. Am. Chem. Soc.* **2004**, *126*, 15046−15047.

(11) Chène, P. Inhibiting the p53−MDM2 interaction: an important target for cancer therapy. *Nat. Rev. Cancer* **2003**, *3*, 102.

(12) Kussie, P. H.; Gorina, S.; Marechal, V.; Elenbaas, B.; Moreau, J.; Levine, A. J.; Pavletich, N. P. Structure of the MDM2 Oncoprotein Bound to the p53 Tumor Suppressor Transactivation Domain. *Science* **1996**, *274*, 948.

(13) Levine, A. J. p53, the Cellular Gatekeeper for Growth and Division. *Cell* **1997**, *88*, 323−331.

(14) Orita, A.; Hasegawa, D.; Nakano, T.; Otera, J. Double Elimination Protocol for Synthesis of 5,6,11,12-Tetradehydrodibenzo-[a,e]cyclooctene. *Chem.—Eur. J.* **2002**, *8*, 2000−2004.

(15) Xu, F.; Peng, L.; Shinohara, K.; Morita, T.; Yoshida, S.; Hosoya, T.; Orita, A.; Otera, J. Substituted 5,6,11,12-Tetradehydrodibenzo-[a,e]cyclooctenes: Syntheses, Properties, and DFT Studies of Substituted Sondheimer−Wong Diynes. *J. Org. Chem.* **2014**, *79*, 11592−11608.

(16) Hu, B.; Gilkes, D. M.; Chen, J. Efficient p53 Activation and Apoptosis by Simultaneous Disruption of Binding to MDM2 and MDMX. *Cancer Res.* **2007**, *67*, 8810.

(17) Phan, J.; Li, Z.; Kasprzak, A.; Li, B.; Sebti, S.; Guida, W.; Schönbrunn, E.; Chen, J. Structure-based Design of High Affinity Peptides Inhibiting the Interaction of p53 with MDM2 and MDMX. *J. Biol. Chem.* **2010**, *285*, 2174−2183.

(18) Brown, C. J.; Quah, S. T.; Jong, J.; Goh, A. M.; Chiam, P. C.; Khoo, K. H.; Choong, M. L.; Lee, M. A.; Yurlova, L.; Zolghadr, K.; Joseph, T. L.; Verma, C. S.; Lane, D. P. Stapled Peptides with Improved Potency and Specificity That Activate p53. *ACS Chem. Biol.* **2013**, *8*, 506−512.

(19) Sharma, K.; Strizhak, A. V.; Fowler, E.; Wang, X.; Xu, W.; Hatt Jensen, C.; Wu, Y.; Sore, H. F.; Lau, Y. H.; Hyvönen, M.; Itzhaki, L. S.; Spring, D. R. Water-soluble, stable and azide-reactive strained dialkynes for biocompatible double strain-promoted click chemistry. *Org. Biomol. Chem.* **2019**, *17*, 8014−8018.

(20) Gordon, C. G.; Mackey, J. L.; Jewett, J. C.; Sletten, E. M.; Houk, K. N.; Bertozzi, C. R. Reactivity of Biarylazacyclooctynones in Copper-Free Click Chemistry. *J. Am. Chem. Soc.* **2012**, *134*, 9199−9208.

(21) Frisch, M. J.; Trucks, G. W.; Schlegel, H. B.; Scuseria, G. E.; Robb, M. A.; Cheeseman, J. R.; Scalmani, G.; Barone, V.; Petersson, G. A.; Nakatsuji, H.; Li, X.; Caricato, M.; Marenich, A. V.; Bloino, J.; Janesko, B. G.; Gomperts, R.; Mennucci, B.; Hratchian, H. P.; Ortiz, J. V.; Izmaylov, A. F.; Sonnenberg, J. L.; Williams; Ding, F.; Lipparini, F.; Egidi, F.; Goings, J.; Peng, B.; Petrone, A.; Henderson, T.; Ranasinghe, D.; Zakrzewski, V. G.; Gao, J.; Rega, N.; Zheng, G.; Liang, W.; Hada, M.; Ehara, M.; Toyota, K.; Fukuda, R.; Hasegawa, J.; Ishida, M.; Nakajima, T.; Honda, Y.; Kitao, O.; Nakai, H.; Vreven, T.; Throssell, K.; Montgomery, J. A., Jr.; Peralta, J. E.; Ogliaro, F.; Bearpark, M. J.; Heyd, J. J.; Brothers, E. N.; Kudin, K. N.; Staroverov, V. N.; Keith, T. A.; Kobayashi, R.; Normand, J.; Raghavachari, K.; Rendell, A. P.; Burant, J. C.; Iyengar, S. S.; Tomasi, J.; Cossi, M.; Millam, J. M.; Klene, M.; Adamo, C.; Cammi, R.; Ochterski, J. W.; Martin, R. L.; Morokuma, K.; Farkas, O.; Foresman, J. B.; Fox, D. J. *Gaussian 09*, Revision D.01; Gaussian Inc.: Wallingford, CT, 2013.

(22) Ess, D. H.; Houk, K. N. Activation Energies of Pericyclic Reactions: Performance of DFT, MP2, and CBS-QB3 Methods for the Prediction of Activation Barriers and Reaction Energetics of 1,3-Dipolar Cycloadditions, and Revised Activation Enthalpies for a Standard Set of Hydrocarbon Pericyclic Reactions. *J. Phys. Chem. A* **2005**, *109*, 9542−9553.

(23) Ess, D. H.; Jones, G. O.; Houk, K. N. Transition States of Strain-Promoted Metal-Free Click Chemistry: 1,3-Dipolar Cycloadditions of Phenyl Azide and Cyclooctynes. *Org. Lett.* **2008**, *10*, 1633−1636.

(24) Zhao, Y.; Truhlar, D. G. The M06 suite of density functionals for main group thermochemistry, thermochemical kinetics, noncovalent interactions, excited states, and transition elements: two new functionals and systematic testing of four M06-class functionals and 12 other functionals. *Theor. Chem. Acc.* **2008**, *120*, 215−241.

https://dx.doi.org/10.1021/acsomega.9b03459
ACS Omega 2020, 5, 1157−1169

(25) Weigend, F.; Ahlrichs, R. Balanced basis sets of split valence, triple zeta valence and quadruple zeta valence quality for H to Rn: Design and assessment of accuracy. *Phys. Chem. Chem. Phys.* **2005**, *7*, 3297−3305.
(26) Simón, L.; Goodman, J. M. How reliable are DFT transition structures? Comparison of GGA, hybrid-meta-GGA and meta-GGA functionals. *Org. Biomol. Chem.* **2011**, *9*, 689−700.
(27) Lam, Y.-h.; Grayson, M. N.; Holland, M. C.; Simon, A.; Houk, K. N. Theory and Modeling of Asymmetric Catalytic Reactions. *Acc. Chem. Res.* **2016**, *49*, 750−762.
(28) Sedgwick, D.; Grayson, M.; Fustero, S.; Barrio, P. Recent Developments and Applications of the Chiral Brønsted Acid Catalyzed Allylboration of Carbonyl Compounds. *Synthesis* **2018**, *50*, 1935−1957.
(29) Chenoweth, K.; Chenoweth, D.; Goddard III, W. A., III Cyclooctyne-based reagents for uncatalyzed click chemistry: A computational survey. *Org. Biomol. Chem.* **2009**, *7*, 5255−5258.
(30) Ess, D. H.; Houk, K. N. Theory of 1,3-Dipolar Cycloadditions: Distortion/Interaction and Frontier Molecular Orbital Models. *J. Am. Chem. Soc.* **2008**, *130*, 10187−10198.
(31) Ess, D. H.; Houk, K. N. Distortion/Interaction Energy Control of 1,3-Dipolar Cycloaddition Reactivity. *J. Am. Chem. Soc.* **2007**, *129*, 10646−10647.
(32) Schoenebeck, F.; Ess, D. H.; Jones, G. O.; Houk, K. N. Reactivity and Regioselectivity in 1,3-Dipolar Cycloadditions of Azides to Strained Alkynes and Alkenes: A Computational Study. *J. Am. Chem. Soc.* **2009**, *131*, 8121−8133.
(33) Taber, D. F.; Jiang, Q.; Chen, B.; Zhang, W.; Campbell, C. L. Synthesis of (−)-Calicoferol B. *J. Org. Chem.* **2002**, *67*, 4821−4827.
(34) Ghera, E.; Maurya, R.; Ben-David, Y. New syntheses of phenanthrenes and of related systems by intramolecular annulation processes. *J. Org. Chem.* **1988**, *53*, 1912−1918.
(35) Wang, Z.-X. An exact mathematical expression for describing competitive binding of two different ligands to a protein molecule. *FEBS Lett.* **1995**, *360*, 111−114.
(36) Lau, Y. H.; de Andrade, P.; McKenzie, G. J.; Venkitaraman, A. R.; Spring, D. R. Linear Aliphatic Dialkynes as Alternative Linkers for Double-Click Stapling of p53-Derived Peptides. *ChemBioChem* **2014**, *15*, 2680−2683.
(37) Barone, V.; Cossi, M. Quantum Calculation of Molecular Energies and Energy Gradients in Solution by a Conductor Solvent Model. *J. Phys. Chem. A* **1998**, *102*, 1995−2001.
(38) Cossi, M.; Rega, N.; Scalmani, G.; Barone, V. Energies, structures, and electronic properties of molecules in solution with the C-PCM solvation model. *J. Comput. Chem.* **2003**, *24*, 669−681.

https://dx.doi.org/10.1021/acsomega.9b03459
ACS Omega 2020, 5, 1157−1169